

# Performance Analysis of LEO Satellite-Based IoT Networks in the Presence of Interference

Ayush Kumar Dwivedi<sup>ID</sup>, *Student Member, IEEE*, Sachin Chaudhari<sup>ID</sup>, *Senior Member, IEEE*,  
Neeraj Varshney<sup>ID</sup>, *Senior Member, IEEE*, Pramod K. Varshney<sup>ID</sup>, *Life Fellow, IEEE*

**Abstract**—This paper explores a star-of-star topology for an internet-of-things (IoT) network using mega low Earth orbit constellations where the IoT users broadcast their sensed information to multiple satellites simultaneously over a shared channel. The satellites use amplify-and-forward relaying to forward the received signal to the ground station (GS), which then combines them coherently using maximal ratio combining. A comprehensive outage probability (OP) analysis is performed for the presented topology. Stochastic geometry is used to model the random locations of satellites, thus making the analysis general and independent of any constellation. The satellites are assumed to be visible if their elevation angle is greater than a threshold, called a mask angle. Statistical characteristics of the range and the number of visible satellites are derived for a given mask angle. Successive interference cancellation (SIC) and capture model (CM)-based decoding schemes are analyzed at the GS to mitigate interference effects. The average OP for the CM-based scheme, and the OP of the best user for the SIC scheme are derived analytically. Simulation results are presented that corroborate the derived analytical expressions. Moreover, insights on the effect of various system parameters like mask angle, altitude, number of satellites and decoding order are also presented. The results demonstrate that the explored topology can achieve the desired OP by leveraging the benefits of multiple satellites. Thus, this topology is an attractive choice for satellite-based IoT networks as it can facilitate burst transmissions without coordination among the IoT users.

**Index Terms**—Amplify-and-forward, LEO satellites, outage probability, satellite-based IoT, stochastic geometry

## I. INTRODUCTION

The upcoming internet-of-things (IoT) networks are expected to connect many devices and sensors with improved battery life and ubiquitous coverage spanning large application scenarios like smart cities, marine IoT, e-healthcare, and connected vehicles. Although terrestrial wireless systems have seen significant enhancements in capacity, coverage at rural and remote locations is still a challenge as estimates suggest that only 25% of the world's landmass has terrestrial connectivity [1]. The intrinsic broadcasting capability of satellite systems makes them a viable solution for delivering truly ubiquitous service to IoT networks often deployed remotely over large areas [2]. A recent 3GPP Rel-17 study-item has also specified the support required for satellite-based

NB-IoT/eMTC networks [3]. Recently, many low Earth orbit (LEO) satellite constellations, e.g., Starlink-SpaceX, OneWeb, Kuiper, Telesat, etc., have been launched. They can potentially serve the remotely deployed IoT networks with multiple LEO satellites in the visible range for a large fraction of the Earth's surface [4]. Moreover, they have relatively low propagation delay at lower powers when compared to the legacy geostationary satellites.

Various architectural issues and enabling solutions related to satellite-based IoT networks have been studied in [5] and [6]. In [5], it is concluded that for satellite-based IoT, relevant upgrades are expected at physical (PHY) and medium access control (MAC) layers to include non-orthogonal and non-pure ALOHA based approaches. According to [6], computationally simple random access schemes and novel topologies need to be explored for massive IoT connectivity.

This paper, therefore, explores a simple star-of-star topology for LEO satellite-based IoT networks, which can facilitate burst transmissions without requiring any synchronization and routing. In the past, star topologies have been used in terrestrial low power wide area network (LPWAN) technologies like Sigfox and long range wide area network (LoRaWAN) but have not been explored for satellite-based IoT networks as done in this paper. The presented results focus on the PHY layer aspects with a particular emphasis on topology and performance analysis.

### A. Related Work

In a star-of-star topology, the access between the node and the relay can be direct or indirect, where the satellites can act as a relay/repeater between the node and the server. However, direct-to-satellite IoT (DtS-IoT) has recently gained traction because of its ease of deployment [7]. In [8], it is shown that LPWAN technologies can be configured for realising DtS-IoT communication. Moreover, some manufacturers' low-cost, battery-powered development kits have also provided the impetus to DtS-IoT using LEO satellites [9]–[11]. The feasibility of DtS-IoT has been established by the link budget analysis carried out on IoT users of various power classes by different companies in a recent 3GPP study-item [3].

In DtS-IoT, the satellites can act as transparent (amplify-and-forward (AF)) or regenerative (decode-and-forward (DF)) relays. The complexity of AF relaying with a fixed gain is less than DF relaying [12], and has been preferred in [3]. The performance of topologies employing AF relaying has been widely studied for various systems. For example, in [13], the performance of a hybrid satellite-terrestrial cooperative

Ayush Kumar Dwivedi (*Corresponding author*) and Sachin Chaudhari are with the Signal Processing and Communication Research Center at International Institute of Information Technology, Hyderabad 500032, India (e-mail: ayush.dwivedi@research.iiit.ac.in; sachin.c@iiit.ac.in).

Neeraj Varshney is with the Wireless Networks Division, National Institute of Standards and Technology, Gaithersburg, MD 20899 USA (e-mail: neerajv@ieee.org).

Pramod K. Varshney is with the Department of Electrical Engineering and Computer Science, Syracuse University, Syracuse, NY 13244 USA (e-mail: varshney@syr.edu).

network consisting of a single relay has been analyzed for generalized fading. In [14], [15], [16], and [17], the performance of an AF system with multiple relays and maximal ratio combining (MRC) at the destination has been analysed for Rayleigh, Nakagami- $m$ , Rician, and shadowed-Rician faded channels, respectively. Additionally, co-channel interference has been included in the performance analysis of relay-based topologies in [18], and [19] for Rayleigh and mixed-Rayleigh-Rician fading channels, respectively. However, this interference can be mitigated using various cancellation techniques. In this context, several interference mitigation techniques for both relay and non-relay systems have also been discussed in the literature. A non-orthogonal multiple access (NOMA) inspired system with a single AF relay and a decoding scheme using the signal from two consecutive time slots is analysed in [20]. Similarly a multi-source, multi-relay system with opportunistic interference cancellation using adaptive AF/DF is analysed in [21]. In both [20] and [21], performance is analysed under the Rayleigh fading assumption. In [22], [23], non-relay terrestrial IoT communication systems have been studied. A LoRaWAN like system with and without fading is considered in [22] and [23], respectively, to show that the capture model (CM) and successive interference cancellation (SIC)-based decoding schemes can perform better than the traditional ALOHA schemes. In CM, the strongest received signal can be decoded successfully despite interference if the signal-to-interference-plus-noise ratio (SINR) is greater than the threshold. Whereas in SIC, decoding is performed in the order of SINRs while cancelling the interference at each step.

Recently many mega-LEO constellations have been launched, and more are being proposed for deployment in the near future. For these, performance analysis done using satellite locations based on their orbit simulations can not be generalized for any new constellation in future. Hence, to generalize the analysis for any constellation, tools from stochastic geometry have been used in recent literature where satellites are assumed to be randomly located around the Earth [24]–[26]. In [24], a theoretical analysis of downlink coverage and rate in a LEO constellation is presented. The satellites are modelled as a binomial point process (BPP) on a sphere, and the users are located on the Earth’s surface. Expressions for statistical characteristics of range and number of visible satellites have been derived along with the notion of an effective number of satellites to suppress the performance mismatch between the practical and random constellations. In [25], coverage and throughput performance for the uplink of a satellite-based-IoT network has been presented using an empirical channel model representing path-loss and large-scale fading. In [26], a fine-grained analysis has been given for the downlink of a LEO satellites-based mmWave relay network. The satellites are assumed to be uniformly distributed on a spherical cap around the Earth, and meta-distribution of the SINR is used for performance evaluation.

## B. Contributions of the paper

Keeping in mind the requirements of IoT, e.g., simple random access, novel topology, and the results from existing literature, this paper explores a star-of-star topology for

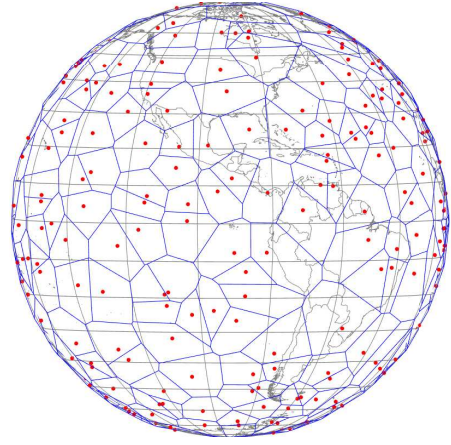


Fig. 1. An example constellation of size  $K = 720$  satellites where the satellites are distributed on a spherical surface following a BPP. The Voronoi diagrams represent the area to which the enclosed satellite is the nearest.

satellite-based IoT networks, which can leverage the benefits of multiple satellites in the visible range. The IoT network is envisioned as the subscriber of one of the many services offered by mega-LEO constellations. The satellites are assumed to be randomly distributed as a BPP on a sphere around the Earth such that a user can see a satellite only if its elevation angle is greater than the mask angle. Multiple satellites simultaneously listen to the broadcast information from multiple IoT users and forward it to the ground station (GS) using fixed-gain AF. It is assumed that IoT users wake up to offload the sensed data to all the visible satellites without any prior coordination and sleep again. This way, the processing is kept simple and energy-efficient for the IoT users, and all the complexity is moved to the satellites and the GS. Since many IoT users are assumed to transmit simultaneously, this work considers CM and SIC-based decoding at the GS.

In [14]–[17], performance analysis was done without considering any interference at the relays as opposed to this paper. Similarly, in [18], [19], although co-channel interference was considered, only a single relay was employed, different from the multiple satellite relay architecture considered in this paper. Neither [23] nor [22] considered a relay system with fading in the propagation environment while analyzing decoding schemes as done in this paper. Moreover, all the above papers neither specifically consider satellites as relays in their performance analysis, nor do they include any information about the location of the sources and relays.

In [24]–[26], the coverage and rate analysis is limited to only single link (either uplink or downlink) performance using a single-serving satellite. Also, no mask elevation angle has been considered to define the visibility of a satellite. In our previous preliminary work [27], a similar topology as this paper was employed, but the analysis was limited to scenarios with single-user and no interference. Compared to [27], the analysis in this work is extended to scenarios with multiple interfering users. Also, in [27], all the visible satellites were considered at fixed locations. However, in this work, the performance of the employed topology is analyzed with different decoding schemes using stochastic geometry to generalize the analysis for any LEO satellite constellation.

The specific contributions of this paper are as follows:

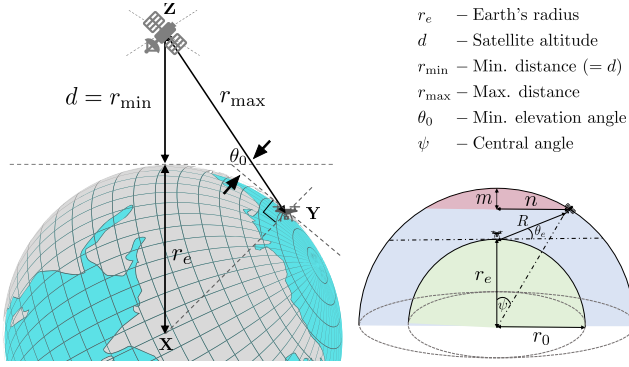


Fig. 2. A geometric representation of the elevation angle  $\theta_e$  and slant range  $R$  between a particular satellite and the IoT user being decoded at GS (maximum slant range  $r_{\max}$  is obtained when  $\theta_e = \theta_0$ ).

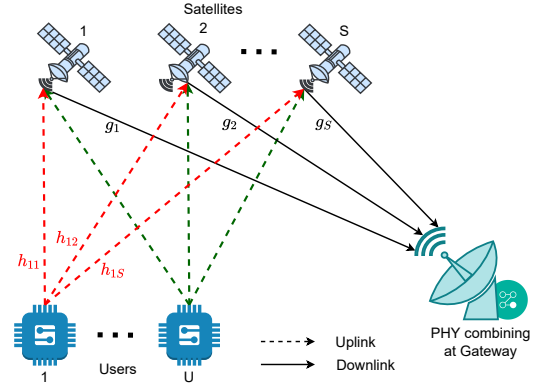


Fig. 3. Schematic diagram of the proposed topology with  $U$  IoT users broadcasting their sensed information to  $S$  visible satellites simultaneously (different colours are used to indicate transmissions from each user). All the satellites forward the signals to the GS using fixed-gain AF relaying.

TABLE I  
SUMMARY OF SYMBOLS AND NOTATIONS

Symbol	Description	Symbol	Description
$U$	Number of IoT users	$S$	Number of satellites used for AF
$K$	Number of satellites in constellation	$K_{\text{vis}}$	Number of visible satellites
$r_e$	Radius of Earth (6371 km)	$d$	Altitude of satellite
$R_{u,s}$	Distance between the $u^{\text{th}}$ user and $s^{\text{th}}$ satellite	$R_g$	Distance between any satellite and GS
$\theta_e$	Elevation angle	$\theta_0$	Minimum elevation angle or mask angle
$P_u$	Transmit power of the $u^{\text{th}}$ user	$P_s$	Transmit power of the $s^{\text{th}}$ satellite
$\sigma_n^2$	AWGN power at satellite for $u^{\text{th}}$ user	$\sigma_w^2$	AWGN power at GS for $s^{\text{th}}$ satellite
$\mathcal{R}$	Target rate	$B$	Available bandwidth
$h_{u,s}$	Channel coefficient of $(u - s)$ user-satellite pair	$g_s$	Channel coefficient of $s^{\text{th}}$ satellite
$m, b, \Omega$	Parameters of Shadowed Rician channel	$\gamma_{\text{th}}$	SINR threshold
$\alpha$	Path loss exponent	$P_{\text{out}}$	Outage probability

- 1) A star-of-star topology is employed for satellite-based IoT networks, which can leverage the benefits of multiple satellites in the visible range.
- 2) The statistical characteristics of the range and the number of visible satellites for a given mask angle are derived in closed form, which is lacking in the existing literature. These characteristics arise from stochastic modelling and are crucial to finding the outage probability (OP).
- 3) The exact expression for the average OP of a user at the GS is derived for CM and the OP for the best user is derived for SIC. The derived theoretical results are validated with Monte-Carlo simulations.
- 4) The effect of various key design parameters like the number of satellites, altitude, elevation angle and user ordering in SIC on the OP are analyzed.

The rest of the paper is organised as follows: Section II presents the detailed system model, and Section III discusses the statistical characteristics of the range and number of visible satellites. The OP derivations for both CM and SIC decoding schemes are derived in Section IV. The results and the associated discussions are presented in Section V, followed by the conclusion in Section VI.

## II. SYSTEM DESCRIPTION

As shown in Fig. 1, a total of  $K$  satellites are assumed to be distributed uniformly around the Earth at an altitude  $d$  km

such that they form a BPP on a sphere of radius  $r_e + d$ , where  $r_e$  is the radius of the Earth. The users are assumed to be located on the Earth's surface. A satellite is considered visible and can receive a signal from a user only if its elevation angle  $\theta_e$  w.r.t user's location is greater than a minimum elevation or mask angle  $\theta_0$ —any satellite for which  $\theta_e < \theta_0$  is considered invisible to the user. As shown in Fig. 2, the distance between a user and a satellite will be minimum when the satellite is at maximum elevation  $\theta_e = 90^\circ$  w.r.t the user. This minimum distance  $r_{\min}$  equals the altitude  $d$  at which all the satellites in the constellation are deployed. Similarly, the distance between a user and a satellite is maximum when the satellite is at an elevation angle  $\theta_e = \theta_0$  w.r.t to the user. The maximum distance for a fixed  $\theta_0$  can be derived as shown in Appendix A. All the notations followed in this paper are defined in Table I.

As shown in Fig. 3, a direct access topology based on a mega-LEO constellation is explored, where  $U$  IoT users communicate their sensed information to a GS via  $S$  satellites among all the  $K_{\text{vis}}$  visible-satellites. The IoT users are assumed to broadcast their information simultaneously using shared resources at the start of every slot as per the slotted-ALOHA scheme similar to the case shown in [28]. Keeping in mind the low complexity of IoT users and design for a common application, it is assumed that all the users transmit at equal power.

The visible satellites amplify and re-transmit the received information to the GS. The GS decodes the information of all the users after coherently combining the signals received from all satellites. Thus, end-to-end communication takes place in two phases. In the first phase, all the IoT users who have sensed information broadcast their signal to all the satellites in the visible range. The signal received at the  $s^{\text{th}}$  satellite can be written as

$$y_s = \sum_{u=1}^U \sqrt{P_u r_{us}^{-\alpha}} h_{us} x_u + n_s, \quad (1)$$

where  $P_u$  is the transmit power of the  $u^{\text{th}}$  IoT user,  $r_{us}$  is the distance between the  $u^{\text{th}}$  user and the  $s^{\text{th}}$  satellite,  $\alpha$  is the path loss exponent,  $x_u$  is the unit energy information signal,  $n_s$  is the additive white Gaussian noise (AWGN) with zero mean and variance  $\sigma_n^2$  at the satellite receiver and  $h_{us}$  is the shadowed-Rician (SR) channel coefficient. The SR model best characterizes the channels which experience line-of-sight (LoS) shadowing and small-scale fading [29]. It is a generalized form of a Rician fading model where the LoS component is assumed to undergo Nakagami- $m$  fading. The SR model is known to fit best the experimental data in the case of characterizing satellite models [29]. For any SR random variable  $h_i$ , the probability density function (PDF) and cumulative distribution function (CDF) of  $H_i = \eta_i |h_i|^2$ , are given, respectively in [30] by

$$f_{H_i}(x) = \alpha_i \sum_{\kappa=0}^{m_i-1} \frac{\zeta(\kappa)}{\eta_i^{\kappa+1}} x^\kappa e^{-\left(\frac{\beta_i - \delta_i}{\eta_i}\right)x}, \quad (2)$$

$$F_{H_i}(x) = 1 - \alpha_i \sum_{\kappa=0}^{m_i-1} \frac{\zeta(\kappa)}{\eta_i^{\kappa+1}} \sum_{p=0}^{\kappa} \frac{\kappa!}{p!} \left(\frac{\beta_i - \delta_i}{\eta_i}\right)^{-(\kappa+1-p)} \times x^p e^{-\left(\frac{\beta_i - \delta_i}{\eta_i}\right)x}, \quad (3)$$

where  $\alpha_i = ((2b_i m_i)/(2b_i m_i + \Omega_i))^{m_i} / 2b_i$ ,  $\beta_i = 1/2b_i$ ,  $\delta_i = \Omega_i/(2b_i)(2b_i m_i + \Omega_i)$  and  $\zeta(\kappa) = (-1)^\kappa (1 - m_i)_\kappa \delta_i^\kappa / (\kappa!)^2$  with  $(\cdot)_\kappa$  being the Pochhammer symbol [31]. Here  $2b_i$  denotes the average power of the multipath component, and  $\Omega_i$  is the average power of the LoS component. The LEO satellites also observe Doppler shifts, but it has not been considered here to keep the analysis simple. It is assumed that the Doppler can be compensated using known techniques [32].

In the second phase, the satellites employ AF to send the received signals to the GS using dedicated orthogonal resources without interference. This assumption considers the downlink between the satellites and GS is resource sufficient. Moreover, it keeps the analysis simple and focused on the effect of uplink, which is limited by the transmit power of the IoT users. Similar to the store-and-forward scheme adopted in [9], it is considered that satellites offload their information when they are nearest to the GS within a time range, i.e.  $r_g = r_{\min}$ . The  $S$  satellites among the  $K_{\text{vis}}$  visible satellites which offload their information to the GS in the defined time range are considered for MRC. The received signal from the  $s^{\text{th}}$  satellite at the GS can be written as

$$z_s = \mathcal{G} \sqrt{r_{\min}^{-\alpha}} g_s \left( \sum_{u=1}^U \sqrt{P_u r_{us}^{-\alpha}} h_{us} x_u + n_s \right) + w_s, \quad (4)$$

where  $g_s$  is the SR channel coefficient between the  $s^{\text{th}}$  satellite and GS,  $\mathcal{G}$  is the AF gain factor and  $w_s$  is the additive white Gaussian noise with zero mean and variance  $\sigma_w^2$  at the GS receiver. Ideally, the effect of the channel between the user and the satellite is equalized by the AF gain factor [12]. In this paper, the received signal is scaled at the satellite by a fixed-gain factor  $\mathcal{G}$ , which is inversely proportional to the total received power and is defined as

$$\mathcal{G} = \sqrt{\frac{P_s}{\sum_{u=1}^U P_u \mathbb{E}[r_{us}^{-\alpha} |h_{us}|^2] + \sigma_n^2}}. \quad (5)$$

The instantaneous end-to-end SINR of the information signal from the  $s^{\text{th}}$  satellite for the  $u^{\text{th}}$  user at the GS can be written as

$$\begin{aligned} \gamma_{us} &= \frac{r_{\min}^{-\alpha} r_{us}^{-\alpha} G_s H_{us}}{r_{\min}^{-\alpha} G_s \left( \sum_{\substack{i=1 \\ i \neq u}}^U r_{is}^{-\alpha} H_{is} + 1 \right) + \frac{P_s}{\mathcal{G}^2 \sigma_n^2}}, \\ &= \frac{r_{us}^{-\alpha} G_s H_{us}}{G_s \left( \sum_{\substack{i=1 \\ i \neq u}}^U r_{is}^{-\alpha} H_{is} + 1 \right) + C}, \end{aligned} \quad (6)$$

where  $H_{us} = \eta_u |h_{us}|^2$  is the instantaneous signal-to-noise ratio (SNR) of a user-satellite link with  $\eta_u = \frac{P_u}{\sigma_n^2}$  and  $G_s = \eta_s |g_s|^2$  is the instantaneous SNR of a satellite-GS link with  $\eta_s = \frac{P_s}{\sigma_w^2}$  and  $C = \frac{P_s}{r_{\min}^{-\alpha} \sigma_n^2 \mathcal{G}^2}$ . Using (5), we can further simplify  $C$  as

$$\begin{aligned} C &= \frac{P_s}{r_{\min}^{-\alpha} \sigma_n^2 \mathcal{G}^2} = \frac{1}{r_{\min}^{-\alpha} \sigma_n^2} \sum_{u=1}^U P_u \mathbb{E}[r_{us}^{-\alpha} |h_{us}|^2] + \sigma_n^2 \\ &= \frac{1}{r_{\min}^{-\alpha}} \left( 1 + \sum_{u=1}^U \mathbb{E}[r_{us}^{-\alpha} H_{us}] \right). \end{aligned} \quad (7)$$

Similar to [33], it is assumed that perfect channel state information (CSI) is available at the GS. It also keeps the analysis focused on the topology. Since the GS combines the signals from all the visible satellites using MRC, the end-to-end SINR of the combined signal for the  $u^{\text{th}}$  user at the GS is given by

$$\gamma_u = \sum_{s=1}^S \gamma_{us}. \quad (8)$$

In this paper, two decoding schemes are compared to analyse the performance of the proposed topology:

- *Capture model (CM)*: The GS is assumed to perfectly decode the information of the desired user out of many interfering signals if its SINR is higher than a threshold. This type of decoding is similar to the capture effect used in LoRa [34].
- *Successive interference cancellation (SIC)*: The GS decodes the information of the intended user by successively removing the information of other users in the order of their SINRs [35]. The user with the highest SINR is decoded first, and its reconstructed signal is subtracted from the received superimposed signal to decode the re-



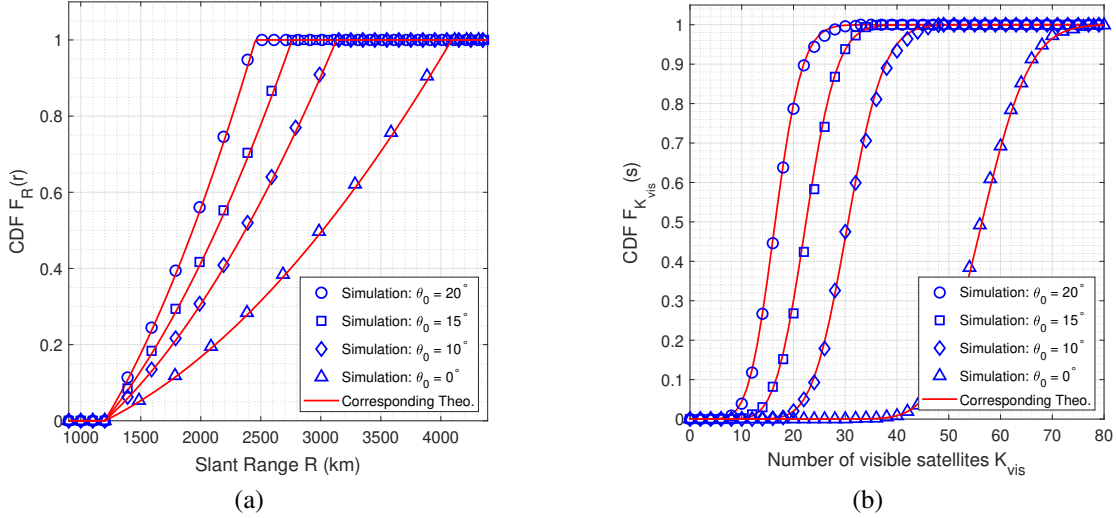


Fig. 4. (a) CDF  $F_R(r)$  of the distance between a user and a visible satellite in the constellation at 1200 km altitude. (b) CDF  $F_{K_{vis}}(s)$  of the number of satellites visible to any user in a constellation of 720 satellites at 1200 km altitude.

maining users. The user with SINR less than the threshold and subsequent users in the order are considered non-decodable and contribute to the outage. As shown in [33], perfect decoding with SIC is considered if the SINR is greater than the threshold to keep the analysis simple.

### III. SLANT DISTANCE AND THE NUMBER OF VISIBLE SATELLITES

Since the satellites are considered to be distributed on a spherical surface following a BPP, the distance between a user and a satellite is random. Moreover, the total number of visible satellites is also random and depends upon  $\theta_0$  and the total number of satellites in the constellation  $K$ . Statistical characteristics of the slant distance and number of visible satellites are derived in this section.

#### A. Statistical characteristics of the distance between the user and the satellite

The CDF of the distance  $R$  between a user and visible satellites in the constellation is given by

$$F_R(r) = \begin{cases} 0, & r < r_{\min} \\ \frac{r^2 - r_{\min}^2}{r_{\max}(\theta_0)^2 - r_{\min}^2}, & r_{\min} \leq r \leq r_{\max}(\theta_0) \\ 1, & r > r_{\max} \end{cases} \quad (9) \quad 0 \leq \theta_0 < 90^\circ$$

and the corresponding PDF is given by

$$f_R(r) = \begin{cases} \frac{2r}{r_{\max}(\theta_0)^2 - r_{\min}^2}, & r_{\min} \leq r \leq r_{\max}(\theta_0) \\ 0, & \text{otherwise} \end{cases} \quad (10) \quad 0 \leq \theta_0 < 90^\circ$$

where  $r_{\min} = d$  is the orbital altitude and  $r_{\max}(\theta_0) = \sqrt{(r_e \sin \theta_0)^2 + (r_e + r_{\min})^2} - r_e \sin \theta_0$  is the maximum distance observed at mask elevation angle  $\theta_0$ . The proofs for

(9) and (10) are provided in Appendix A. The effect of  $\theta_0$  on the range can be inferred from Fig. 4a. It can be observed that the derived expressions match the simulation results. The slant range for which the CDF reaches 1 corresponds to the maximum possible range for a user. As the mask angle increases, the maximum possible range decreases. However, it can be observed that the maximum range decreases rapidly with an increase in the mask angle from  $0^\circ$  to  $10^\circ$  when compared to  $10^\circ$  to  $20^\circ$ . It can be attributed to the fact that,  $r_{\max}$  changes non-linearly with change in  $\theta_0$  as shown in (44).

**Remark:** For the special case of  $\theta_0 = 0^\circ$ ,  $r_{\max}(0^\circ) = \sqrt{r_{\min}^2 + 2r_e r_{\min}}$ . Hence for  $r_{\min} \leq r \leq r_{\max}(0^\circ)$ , (9) and (10) can be simplified as

$$F_{R_0}(r) = \frac{r^2 - r_{\min}^2}{2r_e r_{\min}} \quad (11)$$

$$f_{R_0}(r) = \frac{r}{r_e r_{\min}} \quad (12)$$

where  $R_0$  denotes the random variable for  $R$  at  $\theta_0 = 0^\circ$ . The expressions in (11) and (12) match with the expressions given for the characteristics of the distance in [26], where they are derived for  $\theta_0 = 0^\circ$  only. The simplified expressions shown above are used for scenarios where high-rise structures like mountains and buildings do not mask satellite visibility.

#### B. Statistical characteristics of the number of visible satellites

A satellite is visible to a user only if its elevation angle exceeds the minimum required elevation  $\theta_0$ , also called the mask angle. For a given mask elevation angle  $\theta_0$ , the number of visible satellites  $K_{vis}$  to any user is a binomial random variable with success probability

$$\mathcal{P} = \frac{r_{\max}(\theta_0)^2 - r_{\min}^2}{4r_e(r_e + r_{\min})}, \quad (13)$$

where  $r_{\max}(\theta_0)$  is the distance observed at  $\theta_0$ . The proof for (13) is provided in Appendix B. The effect of mask angle on the number of visible satellites can be inferred from Fig. 4b. It can be observed that the derived expressions match the simulation results. The number of visible satellites for which CDF

$$\begin{aligned}
& F_{\gamma_{us} | r_{us}}(x) \\
&= 1 - \sum_{k_1=0}^{m_{us}-1} \sum_{p=0}^{k_1} \alpha_{us} \frac{k_1! \zeta(k_1)}{p! \eta_{us}^{k_1+1}} A_1^{-(k_1+1-p)} \sum_{k_2=0}^{m_s-1} \alpha_s \frac{\zeta(k_2)}{\eta_s^{k_2+1}} \sum_{z=0}^p \binom{p}{z} \left(\frac{xa}{r_{us}^{-\alpha}}\right)^{p-z} \exp\left[-A_1 \left(\frac{xa}{r_{us}^{-\alpha}}\right)\right] \left(\frac{x C}{r_{us}^{-\alpha}}\right)^z \\
&\quad \times \int_{g=0}^{\infty} g^{-z+k_2} \exp\left[-A_1 \left(\frac{x C}{r_{us}^{-\alpha} g}\right) - A_2 g\right] dg \tag{18}
\end{aligned}$$

$$\begin{aligned}
&= 1 - \sum_{k_1=0}^{m_{us}-1} \sum_{p=0}^{k_1} \alpha_{us} \frac{k_1! \zeta(k_1)}{p! \eta_{us}^{k_1+1}} A_1^{-(k_1+1-p)} \sum_{k_2=0}^{m_s-1} \alpha_s \frac{\zeta(k_2)}{\eta_s^{k_2+1}} \sum_{z=0}^p \binom{p}{z} \left(\frac{xa}{r_{us}^{-\alpha}}\right)^{p-z} \exp\left[-A_1 \left(\frac{xa}{r_{us}^{-\alpha}}\right)\right] \left(\frac{x C}{r_{us}^{-\alpha}}\right)^z \\
&\quad \times 2 \left(\frac{A_1 x C}{A_2 r_{us}^{-\alpha}}\right)^{(1-z+k_2)/2} K_{1-z+k_2} \left(2 \sqrt{\frac{A_1 A_2 x C}{r_{us}^{-\alpha}}}\right) \tag{19}
\end{aligned}$$

equals 1 denotes the maximum possible number of satellites which can be visible to a user. As the mask angle increases, the surface area of the cap region shown in Fig. 2 decreases, and so does the maximum number of visible satellites. It can be observed that the maximum possible number of visible satellites decreases rapidly from  $0^\circ$  to  $10^\circ$  when compared to  $10^\circ$  to  $20^\circ$ . It can be understood using (44) and (50), since  $A_{\text{vis}}$  decreases non-linearly with an increase in  $\theta_e$ .

**Remark:** With  $\mathcal{P}_0$  denoting the success probability for the special case of  $\theta_0 = 0^\circ$ , (13) can be simplified as

$$\mathcal{P}_0 = \frac{r_{\min}}{2(r_e + r_{\min})}. \tag{14}$$

#### IV. OUTAGE PROBABILITY ANALYSIS

The outage probability of a particular user is defined as

$$\begin{aligned}
P_{\text{out}}(\mathcal{R}) &\triangleq \mathbb{P}\left[\frac{B}{2} \log_2(1 + \text{SINR}) \leq \mathcal{R}\right] \\
&= \mathbb{P}[\text{SINR} \leq \gamma_{\text{th}}], \tag{15}
\end{aligned}$$

where  $\mathcal{R}$  is the target rate,  $B$  is the bandwidth,  $\gamma_{\text{th}} \triangleq 2^{2\mathcal{R}/B} - 1$  is the threshold and SINR needs to be calculated for CM and SIC schemes separately.

##### A. OP for CM based decoding

In CM based decoding, a user is decoded in the presence of interference from all other users. Hence the OP of a user at the GS can be written as

$$\begin{aligned}
P_{\text{out}}(\mathcal{R}) &= \mathbb{P}[\gamma_u \leq \gamma_{\text{th}}] \times \mathbb{P}[K_{\text{vis}} \geq S] \\
&= F_{\gamma_u}(\gamma_{\text{th}}) \left[1 - \sum_{j=0}^{S-1} \binom{K}{j} \mathcal{P}^j (1 - \mathcal{P})^{K-j}\right], \tag{16}
\end{aligned}$$

where  $\gamma_u = \sum_{s=1}^S \gamma_{us}$ . The following three-step approach has been followed to find the exact expression for (16).

- 1) Finding the CDF of  $\gamma_{us}$  conditioned on  $r_{us}$  for a single satellite scenario.
- 2) Finding the moment generating function (MGF) of  $\gamma_{us}$  and  $\gamma_u$  for extending the analysis to the multi-satellite scenario.
- 3) Finding the CDF of  $\gamma_u$  and consequently the OP in multi-satellite scenario.

*Step 1:* Using the theorem of transformation of random variables, the CDF of  $\gamma_{us}$  conditioned on the distance between the user and the satellite can be found as

$$\begin{aligned}
& F_{\gamma_{us} | r_{us}}(x) \\
&= \mathbb{P}[\gamma_{us} < x | r_{us}] \\
&= \mathbb{P}\left[\frac{r_{us}^{-\alpha} G_s H_{us}}{G_s \left(\left\{\sum_{i=1, i \neq u}^U r_{is}^{-\alpha} H_{is}\right\} + 1\right) + C} \leq x \mid r_{us}\right] \\
&\stackrel{(i)}{\approx} \mathbb{P}\left[\frac{r_{us}^{-\alpha} G_s H_{us}}{G_s ((U-1)\bar{I} + 1) + C} \leq x \mid r_{us}\right] \\
&\stackrel{(ii)}{=} \int_{g=0}^{\infty} F_{H_{us}}\left(\frac{xa}{r_{us}^{-\alpha}} + \frac{x C}{r_{us}^{-\alpha} g}\right) f_{G_s}(g) dg, \tag{17}
\end{aligned}$$

where in (i), interference from a user is approximated as  $\bar{I} = \mathbb{E}[r_{is}^{-\alpha} H_{is}]$  for mathematical tractability and in (ii),  $a = ((U-1)\bar{I} + 1)$  for convenience. An expression for the term  $\mathbb{E}[r_{is}^{-\alpha} H_{is}]$  is derived in Appendix C. Using (2), (3), with the knowledge of binomial expansion and interchanging the order of summation and integration, (17) can be simplified as (18), where  $A_1 = \frac{\beta_{us} - \delta_{us}}{\eta_{us}}$  for uplink and  $A_2 = \frac{\beta_s - \delta_s}{\eta_s}$  for downlink. The integral expression in (18) can be solved using [31, Eq. 3.471.9] to get the closed-form expression for  $F_{\gamma_{us} | r_{us}}(x)$  as shown in (19), where  $K_\nu(\cdot)$  is the  $\nu^{\text{th}}$  order modified Bessel function of second kind.

*Step 2:* For any random variable  $X$ , with MGF  $M_X(t)$  and  $\mathcal{L}\{\cdot\}$  denoting the Laplace transform operator, we can write

$$\begin{aligned}
\mathcal{L}\{f_X(x)\} &= M_X(-t), \\
\mathcal{L}\{F_X(x)\} &= \frac{M_X(-t)}{t}, \tag{20}
\end{aligned}$$

where (20) follows from the integral property of Laplace transform. Therefore, flipped MGF,  $M_X(-t)$  is required to obtain CDF by applying the inverse Laplace transform on (20). The flipped MGF (referred simply as MGF hereafter) of  $\gamma_{us}$  conditioned on  $r_{us}$  can be derived using the definition of the Laplace transform as

$$M_{\gamma_{us} | r_{us}}(-t) = 1 - t \int_{x=0}^{\infty} e^{-tx} (1 - F_{\gamma_{us} | r_{us}}(x)) dx. \tag{21}$$

$$\begin{aligned}
M_{\gamma_{us} | r_{us}}(-t) &= 1 - t \sum_{k_1=0}^{m_{us}-1} \sum_{p=0}^{k_1} \alpha_{us} \frac{k_1! \zeta(k_1)}{p! \eta_{us}^{k_1+1}} A_1^{-(k_1+1-p)} \sum_{k_2=0}^{m_s-1} \alpha_s \frac{\zeta(k_2)}{\eta_s^{k_2+1}} \sum_{z=0}^p \binom{p}{z} (a r_{us}^\alpha)^{p-z} (C r_{us}^\alpha)^{(1+z+k_2)/2} \\
&\quad \times \left( \frac{A_1}{A_2} \right)^{(1-z+k_2)/2} \epsilon^{-\mu} \exp \left[ \frac{\lambda^2}{2\epsilon} \right] \frac{\Gamma(\mu + \nu + \frac{1}{2}) \Gamma(\mu - \nu + \frac{1}{2})}{\lambda} W_{-\mu, \nu} \left( \frac{\lambda^2}{\epsilon} \right)
\end{aligned} \quad (22)$$

Using (19) and [31, Eq. 6.643.3], the integral in (21) can be solved to arrive at the closed-form expression for  $M_{\gamma_{us} | r_{us}}(-t)$  as shown in (22), where

$$\begin{aligned}
\mu &= p + 1 + \frac{k_2 - z}{2}, \\
\epsilon &= A_1 a r_{us}^\alpha + t, \\
\lambda &= \sqrt{A_1 A_2 C r_{us}^\alpha}, \\
\nu &= \frac{1 - z + k_2}{2},
\end{aligned}$$

and  $\Gamma(\cdot)$ ,  $W_{\mu, \nu}(\cdot)$  are the Gamma and Whittaker functions, respectively.

The MGF of  $\gamma_{us}$  can be calculated by averaging over  $r_{us}$  using (10) and (22) as

$$\begin{aligned}
M_{\gamma_{us}}(-t) &= \int_{r_{\min}}^{r_{\max}} M_{\gamma_{us} | r_{us}}(-t) f_R(r_{us}) dr_{us} \\
&= \frac{2}{r_{\max}^2 - r_{\min}^2} \int_{r_{\min}}^{r_{\max}} r_{us} M_{\gamma_{us} | r_{us}}(-t) dr_{us}. \quad (23)
\end{aligned}$$

The integral in (23) can be efficiently evaluated using numerical techniques as discussed in Appendix D.

The MRC is implemented at the GS on the signal with end-to-end SINR as defined in (8). Since all the  $S$  satellite-GS links are independent, the MGF of the end-to-end SINR can be written as

$$M_{\gamma_u}(-t) = \prod_{s=1}^S M_{\gamma_{us}}(-t) \quad (24)$$

Step 3: Using (20), the CDF of  $\gamma_u$  as be obtained as

$$F_{\gamma_u}(x) = \mathcal{L}^{-1} \left\{ \frac{M_{\gamma_u}(-t)}{t} \right\} (x). \quad (25)$$

The inverse Laplace transform in (25) can be efficiently calculated using the numerical technique presented in [36] as

$$\begin{aligned}
F_{\gamma_u}(x) &= \frac{2^{-Q} e^{D/2}}{x} \sum_{q=0}^Q \binom{Q}{q} \\
&\quad \sum_{n=0}^{N+q} \frac{(-1)^n}{\Delta_n} \Re \left\{ \frac{M_{\gamma_u} \left( -\frac{D + 2\pi j n}{2x} \right)}{\frac{D + 2\pi j n}{2x}} \right\} \\
&\quad + E(D, Q, N), \quad (26)
\end{aligned}$$

where

$$\Delta_n = \begin{cases} 2, & n = 0 \\ 1, & n = 1, 2, \dots, N \end{cases}$$

and

$$\begin{aligned}
E(D, Q, N) &= \frac{e^{-D}}{1 - e^{-D}} + \frac{2^{-Q} e^{D/2}}{x} \sum_{q=0}^Q (-1)^{N+1+q} \binom{Q}{q} \\
&\quad \Re \left\{ \frac{M_{\gamma_u} \left( -\frac{D + 2\pi j (N + q + 1)}{2x} \right)}{\frac{D + 2\pi j (N + q + 1)}{2x}} \right\}.
\end{aligned}$$

The values of  $D$ ,  $Q$  and  $N$  are selected to keep the discretization and truncation errors negligible. Thus, using (13) and (26) in (16), completes the derivation of OP for CM-based decoding.

### B. OP for SIC based decoding

SIC is an ordering-based scheme where the GS decodes the information of users in the order of their end-to-end SINRs. For the ease of understanding,  $l \in [1, U]$  is used to denote the order/iteration of SIC decoding and  $\mathbf{D}[l]$  is used to denote the set of indexes for all decoded users till the  $l^{\text{th}}$  iteration. Additionally,  $\mathbf{D}\{l\}$  is used to denote the index of the user decoded at the  $l^{\text{th}}$  iteration. Therefore end-to-end SINR of the signal from  $u^{\text{th}}$  user received via  $s^{\text{th}}$  satellites in the  $l^{\text{th}}$  iteration of SIC decoding can be written as

$$\gamma_{us}^{(l)} = \frac{r_{us}^{-\alpha} G_s H_{us}}{G_s ((U-l)\bar{I} + 1) + C} \quad \forall u \notin \mathbf{D}[l-1]. \quad (27)$$

Also, the end-to-end SINR of the MRC combined signal of the  $u^{\text{th}}$  user can be written as

$$\gamma_u^{(l)} = \sum_{s=1}^S \gamma_{us}^{(l)} \quad \forall u \notin \mathbf{D}[l-1]. \quad (28)$$

At every iteration, the user with the highest SINR is decoded such that

$$\gamma_{\mathbf{D}\{l\}}^{(l)} = \begin{cases} \max_u \gamma_u^{(l)}, & l = 1 \\ \max_{u, u \notin \mathbf{D}[l-1]} \gamma_u^{(l)}, & \gamma_{\mathbf{D}\{l-1\}}^{(l-1)} > \gamma_{\text{th}}, l > 1 \\ 0, & \text{otherwise,} \end{cases} \quad (29)$$

where the set of indexes for all the decoded users is updated after every iteration as

$$\mathbf{D}[l-1] = \begin{cases} \emptyset, & l = 1 \\ \mathbf{D}[l-2] \cup \left\{ \arg \max_{u, u \notin \mathbf{D}[l-2]} \gamma_u^{(l-1)} \right\}, & \gamma_{\mathbf{D}\{l-1\}}^{(l-1)} > \gamma_{\text{th}}, l > 1 \\ \mathbf{D}[l-2], & \gamma_{\mathbf{D}\{l-1\}}^{(l-1)} \leq \gamma_{\text{th}}, l > 1. \end{cases} \quad (30)$$

$$F_{\tilde{H}_{us}}(z) = \int_{r_{\min}}^{r_{\max}} F_{H_{us}}\left(\frac{z}{r_{us}^\alpha}\right) f_R(r_{us}) dr_{us} = 1 - \frac{2\alpha_{us}}{r_{\max}^2 - r_{\min}^2} \sum_{k=0}^{m_{us}-1} \sum_{p=0}^k \frac{k! \zeta(k)}{p! \eta_{us}^{k+1}} A^{-(k+1-p)} \int_{r_{\min}}^{r_{\max}} (z r_{us}^\alpha)^p \exp[-Az r_{us}^\alpha] r_{us} dr_{us} \quad (34)$$

$$= 1 - \frac{2}{r_{\max}^2 - r_{\min}^2} \sum_{k=0}^{m_{us}-1} \sum_{p=0}^k \alpha_{us} \frac{k! \zeta(k)}{p! \eta_{us}^{k+1}} A^{-(k+1-p)} \left( \frac{\gamma(V, \rho r_{\max}^\alpha) - \gamma(V, \rho r_{\min}^\alpha)}{\alpha \rho^V} \right) z^p \quad (35)$$

$$M_{\gamma_{us}^{(1)}|G_s}(-t) = 1 - \frac{2t}{r_{\max}^2 - r_{\min}^2} \sum_{k=0}^{m_{us}-1} \sum_{p=0}^k \frac{\alpha_{us}}{\alpha} \frac{k! \zeta(k)}{p! \eta_{us}^{k+1}} A^{-(k-p+V+1)} \left( a + \frac{C}{g_s} \right)^{p-V} \times \int_{x=0}^{\infty} e^{-tx} x^{p-V} \left\{ \gamma\left(V, A r_{\max}^\alpha \left( a + \frac{C}{g_s} \right) x\right) - \gamma\left(V, A r_{\min}^\alpha \left( a + \frac{C}{g_s} \right) x\right) \right\} dx \quad (37)$$

$$= 1 - \frac{2t}{r_{\max}^2 - r_{\min}^2} \sum_{k=0}^{m_{us}-1} \sum_{p=0}^k \frac{\alpha_{us}}{\alpha} \frac{k! \zeta(k)}{p! \eta_{us}^{k+1}} A^{-(k-p+V+1)} \left( a + \frac{C}{g_s} \right)^{p-V} \frac{\Gamma(p+1)}{V} \times \left\{ \frac{[v_1(g_s)]^V}{[v_1(g_s) + t]^{p+1}} {}_2F_1\left(1, p+1; V+1; \frac{v_1(g_s)}{v_1(g_s) + t}\right) - \frac{[v_2(g_s)]^V}{[v_2(g_s) + t]^{p+1}} {}_2F_1\left(1, p+1; V+1; \frac{v_2(g_s)}{v_2(g_s) + t}\right) \right\} \quad (38)$$

Therefore the OP of  $l^{\text{th}}$  user in case of SIC can be written as as:

$$P_{\text{out}}^{(l)}(\mathcal{R}) = \begin{cases} \mathbb{P}[\max_u \gamma_u^{(l)} \leq \gamma_{\text{th}}] \mathbb{P}[K_{\text{vis}} \geq S] & , l = 1 \\ \left\{ \mathbb{P}[\gamma_{\mathbf{D}\{l\}}^{(l)} \leq \gamma_{\text{th}} | \gamma_{\mathbf{D}\{l-1\}}^{(l-1)} > \gamma_{\text{th}}] (1 - P_{\text{out}}^{(l-1)}(\mathcal{R})) \right. \\ \left. + P_{\text{out}}^{(l-1)}(\mathcal{R}) \right\} \mathbb{P}[K_{\text{vis}} \geq S] & , l > 1, \end{cases} \quad (31)$$

$$F_{\gamma_{us}^{(1)}|G_s} = \mathbb{P}\left[ \frac{r_{us}^{-\alpha} G_s H_{us}}{G_s ((U-1)\bar{I} + 1) + C} \leq x \mid G_s \right] = \mathbb{P}\left[ r_{us}^{-\alpha} H_{us} \leq ax + \frac{Cx}{G_s} \mid G_s \right] = F_{\tilde{H}_{us}|G_s}\left(ax + \frac{Cx}{g_s}\right), \quad (33)$$

or simply as

$$P_{\text{out}}^{(l)}(\mathcal{R}) = F_{\gamma_u^{(l)}|\gamma_{\text{th}}} \left[ 1 - \sum_{j=0}^{S-1} \binom{K}{j} \mathcal{P}^j (1 - \mathcal{P})^{K-j} \right]. \quad (32)$$

The exact expression of (32) for  $l = 1$  can be obtained. However, for  $l > 1$  it is not mathematically tractable since the distribution of  $\gamma_{\mathbf{D}\{l\}}^{(l)}$  conditioned on  $\gamma_{\mathbf{D}\{l-1\}}^{(l-1)} > \gamma_{\text{th}}$  is difficult to obtain. Therefore, the exact expression for OP in case of SIC is obtained for the best user ( $l = 1$ ) only, which is a lower bound on the average OP of the system and simulation results are presented for  $l > 1$ . For the case of  $l = 1$ , distribution for maximum of dependent random variables  $\gamma_u^{(1)}$  is required. Hence the derivation is done using the following steps:

- 1) Finding the CDF of  $\gamma_{us}^{(1)}$  conditioned on  $G_s$  for single satellite scenario.
- 2) Finding the MGF of  $\gamma_{us}^{(1)}$  and  $\gamma_u^{(1)}$  conditioned on  $G_s$  for extending the analysis to multi-satellite scenario.
- 3) Finding the CDF and consequently the OP for  $\max_u \gamma_u^{(1)}$  averaged over all  $G_s$ .

*Step 1:* Using the theorem of transformation of random variables, the CDF of  $\gamma_{us}^{(1)}$  conditioned on  $G_s$  can be written

where  $a = ((U-1)\bar{I} + 1)$  and  $\tilde{H}_{us} = r_{us}^{-\alpha} H_{us}$ . The CDF  $F_{\tilde{H}_{us}}(z)$  can be written as (34) where the integral can be solved using [31, Eq. 3.381.8] to obtain (35). In (35),  $A = \frac{\beta-\delta}{\eta}$ ,  $V = \frac{\alpha p+2}{\alpha}$ ,  $\rho = Az$  and  $\gamma(\cdot, \cdot)$  is the lower incomplete Gamma function.

*Step 2:* Similar to the approach followed in the derivation of CM decoding, the MGF of  $\gamma_{us}^{(1)}$  conditioned on  $G_s$  can be written as

$$M_{\gamma_{us}^{(1)}|G_s}(-t) = 1 - t \int_{x=0}^{\infty} e^{-tx} \left( 1 - F_{\tilde{H}_{us}|G_s}\left(ax + \frac{Cx}{g_s}\right) \right) dx. \quad (36)$$

Rearranging the terms, (36) can be written as (37). The integral in (37) can be solved using [31, Eq. 6.455.2] to obtain (38), where

$$v_1(g_s) = A r_{\max}^\alpha \left( a + \frac{C}{g_s} \right), \quad (39)$$

$$v_2(g_s) = A r_{\min}^\alpha \left( a + \frac{C}{g_s} \right), \quad (40)$$

and  ${}_2F_1(\cdot)$  is the Gauss hypergeometric function. Since all the  $S$  satellites-GS links are independent, the MGF of  $\gamma_u^{(1)}$  conditioned on  $G_s$  can therefore be written as

$$M_{\gamma_u^{(1)}|G_s}(-t) = \prod_{s=1}^S M_{\gamma_{us}^{(1)}|G_s}(-t) \quad (41)$$



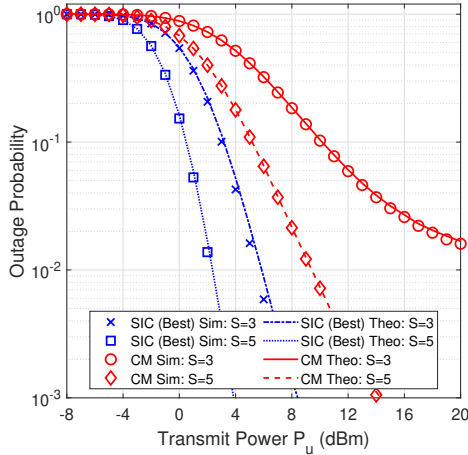


Fig. 5. Validation of theoretical and simulation results: OP vs transmit power  $P_u$  in both SIC and CM for  $U = 5$  and different number of satellites  $S$ .

*Step 3:* Using (20) and averaging over all the  $G_s$ , the CDF of  $\max_u \gamma_u^{(1)}$  can be derived as

$$F_{\gamma_u^{(1)}}(x) = \int_{g_1} \cdots \int_{g_S} \left[ \mathcal{L}^{-1} \left\{ \frac{M_{\gamma_u^{(1)}|G_s}(-t)}{t} \right\} (x) \right]^U \times \left\{ \prod_{s=1}^S f_{G_s}(g_s) \right\} dg_1 \cdots dg_S. \quad (42)$$

The integral in (42) can be efficiently evaluated using numerical techniques similar to the ones discussed in Appendix D. Thus, using (13) and (42) in (32) with  $l = 1$  completes the derivation of the OP in SIC decoding for best user.

## V. RESULTS

This section presents simulation and theoretical results derived in this work to get useful insights into the system. Initially, the theoretical analysis is validated with the simulation results. Later the effect of various system parameters on OP performance is analyzed. Since many parameters affect the performance, an attempt is made to understand them one by one by keeping all other parameters constant. All the simulations and plots have been realised using MATLAB. The parameters  $(m, b, \Omega)$  of SR fading under heavy and average shadowing conditions are considered to be  $(2, 0.063, 0.0005)$  and  $(5, 0.251, 0.279)$ , respectively [37]. The default parameters for simulations, unless stated otherwise are: constellation size = 720, constellation altitude  $h = 1200$  km, radius of the Earth  $r_e = 6371$  km, mask elevation angle  $\theta_0 = 10^\circ$ , transmit power of the satellite  $P_s = 10$  W, noise power at the GS  $\sigma_w^2 = -98$  dBm, target rate = 10 kbps, bandwidth = 125 kHz, path loss exponent  $\alpha = 2$  and number of channel realizations =  $10^5$ . Also while computing the numerical Laplace inverse as in (26),  $D = 10 \ln(10)$ ,  $N = 21$  and  $Q = 15$  is used to maintain the discretization and truncation error less than  $10^{-10}$  which is negligible compared to the range of derived OP.

### A. Validation of theoretical and simulation results

Fig. 5 shows the average OP vs transmit power  $P_u$  for  $U = 5$  users in the case of  $S = 3$  and  $S = 5$  satellites.

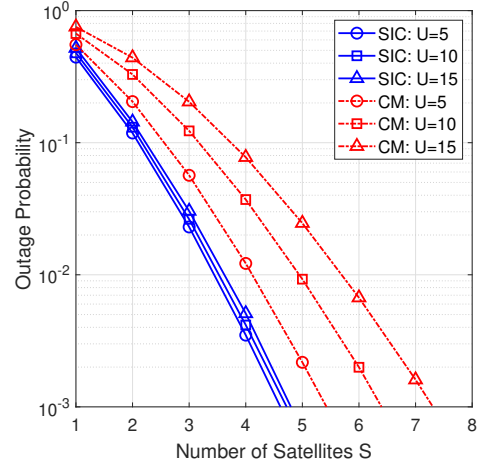


Fig. 6. Effect of number of satellites  $S$ : Averaged OP vs  $S$  in both SIC and CM at  $P_u = 4$  dB and different number of users  $U$ .

The OP for every user in the order of their SINRs has been calculated and then averaged to obtain the average OP of the system. It is observed that the average OP derived theoretically using the approximation is very close to the simulation results for both CM and SIC based decoding. This validates the correctness of the derivation presented in Section IV-A and Section IV-B. Only simulation results are presented in further results to maintain the brevity of the paper.

Two more observations can be made from Fig. 5. First, the OP per user decreases with an increase in transmit power of the IoT users. An IoT user's feasible transmit power range from 4 dB to 20 dB can achieve OP ranging from  $10^{-1}$  to  $10^{-3}$  in SIC. Second, as the transmit power increases, the interference effect starts dominating, thus leading to the performance difference between SIC and the CM decoding. However, with an increase in the number of satellites, the OP decreases sharply. Hence leveraging the benefits of multiple visible satellites from an LEO constellation, transmit power of 14-16 dB can achieve an OP of  $10^{-3}$  in a 5 satellite, 5 user system.

### B. Effect of the number of satellites $S$

Fig. 6 shows the OP as a function of number of satellites  $S$  for  $U = 5, 10$  and  $15$  users at  $P_u = 4$  dBm. It is observed that for a fixed number of users, as the number of satellites increases, the OP decreases sharply. It can be observed that merely an addition of 3 satellites can reduce the OP from  $10^{-1}$  to  $10^{-3}$  in both CM and SIC decoding. This also clearly demonstrates how the IoT users can leverage multiple visible satellites of the constellation to enhance system performance. Additionally, it is interesting to note that the OP for 15 users case in SIC is less than the OP for 5 users case in CM.

### C. Effect of the number of users $U$

Fig. 7 shows the impact on the OP as a function of number of users  $U$  at  $P_u = 4$  dBm for  $S = 2, 3$  and  $4$ . It can be observed that the OP increases with an increase in the number of users due to the increase in interference. It can also be observed that the performance gap between the SIC and CM

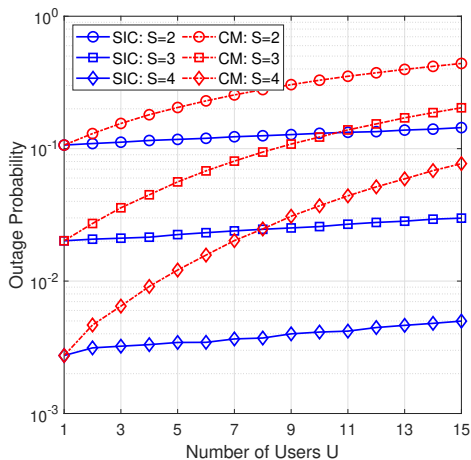


Fig. 7. Effect of number of users  $U$ : Average OP vs  $U$  for both SIC and CM scheme at  $P_u = 4$  dB and different values of satellites  $S$ .

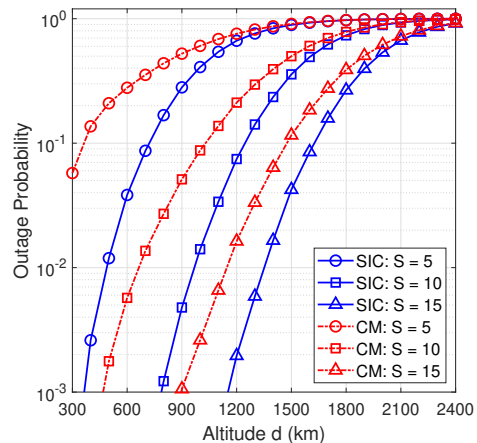


Fig. 8. Effect of altitude  $d$ : Average OP vs  $d$  for both SIC and CM at  $P_u = 4$  dB,  $U = 15$  and different values of satellites  $S$ .

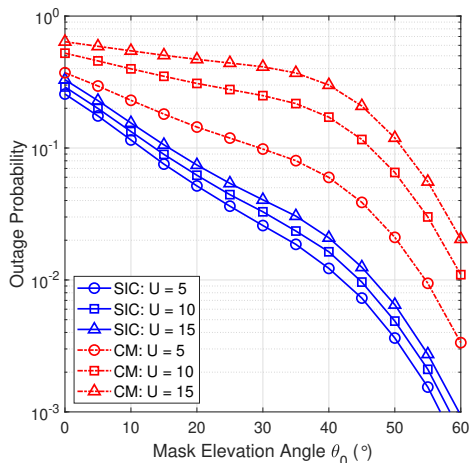


Fig. 9. Effect of mask elevation angle  $\theta_0$ : OP vs  $\theta_0$  for both SIC and CM at  $P_u = 4$  dB,  $S = 3$  and different number of users  $U$

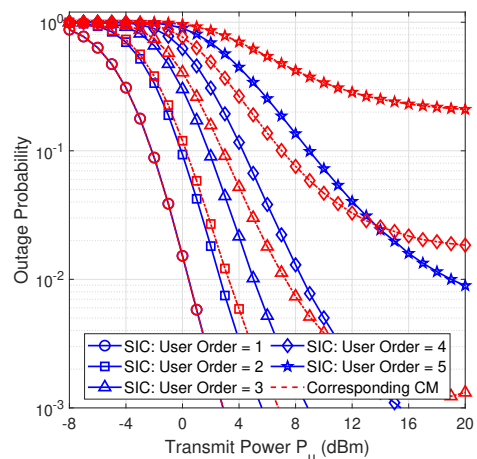


Fig. 10. Effect of decoding order  $l$ : OP vs transmit power  $P_u$  for ordered decoding in both SIC and CM for  $U = 5$  and  $S = 2$

also increases with an increase in  $U$ . This can be attributed to the fact that the impact of interference decreases with decoding of subsequent users in SIC whereas CM assumes a constant number of interferers for all the users. It is interesting to note that the difference between the performance of SIC and CM becomes significant as more and more satellites are added to the system.

#### D. Effect of altitude $d$

Fig. 8 shows the impact of altitude on the OP for  $S = 5, 10$  and  $15$  satellites and  $U = 15$  users at  $P_u = 4$  dBm. It can be observed that OP increases as the altitude increases. This is because the constellation's altitude directly impacts the path loss observed by the signals. It can also be observed that while more satellites enhance the OP performance because of better elevation angles, the benefit of adding more satellites diminishes rapidly with increasing altitude. Hence, the number of satellites and the selection of decoding scheme can be traded-off with the altitude and number of users.

Usually, the LEO satellites are considered to be placed between 600 km to 1800 km. Hence for a desired OP at

a fixed transmit power, Fig. 8 can be used to determine the minimum number of satellites required in look angle for various constellations at different altitudes. For example, using SIC, in a network of 15 active users, a minimum of 15 satellites at 1150 km are required to achieve an OP of  $10^{-3}$ . A similar performance can be achieved with 10 satellites only if placed at an altitude of 800 km.

#### E. Effect of mask elevation angle $\theta_0$

Fig. 9 shows the effect of  $\theta_0$  on OP for  $S = 3$  satellites and  $U = 5, 10$  and  $15$  users at  $P_u = 4$  dBm. The OP decreases with an increase in  $\theta_0$ ; however, the rate of decrease changes at around  $\theta_e = 40^\circ$  for the shown case of  $S = 3$ . It can be explained by the two-fold impact of  $\theta_0$  on the OP. As evident from (44) and (50),  $A_{\text{vis}}$  decreases with an increase in  $\theta_0$ . Hence the probability of seeing a defined number of satellites decreases with an increase in  $\theta_0$  for every user. It, therefore, tends to increase the OP. On the other hand, as evident from (57), an increase in  $\theta_0$  decreases the distance and, consequently, the average path loss between the users and the satellites. It, therefore, tends to reduce the OP. The

impact of reducing path loss dominates nearly till  $\theta_0 = 40^\circ$ . However, after that, the reduced probability of seeing a defined number of satellites rapidly decreases the OP.

#### F. Effect of decoding order $l$ and trade-offs

Fig. 10 shows the OP for various users in ordered decoding, where user 1 means the first user being decoded in SIC. Similarly, in a 5-user scenario, user 5 means the last user decoded in SIC. The OP for corresponding CM has also been shown in Fig. 10 where the user order is solely determined by the SINRs without removing interference for any user. It can be observed that the initial few users in the order have similar OP for both SIC and CM. It can be attributed to the fact that the interference in both SIC and CM remains nearly similar for the initial few users. However, for higher order decoding in SIC, the interference decreases significantly due to the subtraction of information signals of the decoded user. This is not the case in CM; decoding of higher order users happens in heavy interference from users with better channel conditions. Hence the difference between the OP performance of SIC and CM increases significantly for higher-order users. It can be concluded that trading off with the throughput and desired OP, the initial few users can be decoded using CM only, thus reducing the decoding complexity. However, for applications requiring decoding of all or most users, SIC is preferable to CM.

## VI. CONCLUSION

This paper presented a simple and energy-efficient direct-access topology for LEO satellites based IoT networks. The OP performance of the topology was analysed using stochastic geometry to model the random satellite locations. In this context, analytical expressions were derived for average OP in the CM decoding scheme, and the OP of the best user was derived for the SIC decoding scheme. Although all the IoT users transmit at the same power, it was found that the SIC decoding scheme performs better than the CM decoding scheme. The theoretical analysis was verified through rigorous simulations. The effects of system parameters like the number of users, number of satellites, altitude, and mask elevation angle of the constellation on the OP performance were discussed in detail. The results of this paper demonstrate that for the practical values of the above system parameters, the topology is feasible and attractive for low-powered IoT networks.

### APPENDIX A PROOF FOR CDF AND PDF OF $R$

The distribution of  $R$  can be found in three steps:

- 1) Finding  $r_{\min}$ ,  $r_{\max}$  and the relationship between  $R$  and the the surface area of the spherical cap,  $A_{\text{cap}}$  formed by the satellites at the distance less than or equal to  $R$
- 2) Finding the distribution of  $A_{\text{cap}}$
- 3) Finding the distribution of  $R$  from the distribution of  $A_{\text{cap}}$

*Step 1:* From basic geometry as shown in Fig. 2,  $r_{\min} = d$  is the orbital altitude, observed at  $\theta_e = 90^\circ$ . Also,  $r_{\max}(\theta_0)$  will be observed at the mask elevation angle  $\theta_0$ . Hereafter it

is written as simply  $r_{\max}$  to maintain brevity. Applying law-of-cosines for triangles at  $\angle XYZ$  gives,

$$(r_e + r_{\min})^2 = r_e^2 + r_{\max}^2 - 2r_e r_{\max} \cos(90 + \theta_0). \quad (43)$$

Solving the quadratic equation (43) for  $r_{\max}$  and considering all the distances to be positive, we get

$$r_{\max} = \sqrt{(r_e \sin \theta_0)^2 + (r_e + r_{\min})^2 - r_e^2} - r_e \sin \theta_0 \quad (44)$$

Further derivation to find the relationship between  $A_{\text{cap}}$  and  $R$  can be done on similar lines of [24]. From Fig. 2 where  $m$  and  $n$  are shown, we can write

$$A_{\text{cap}} = \pi(m^2 + n^2), \quad (45)$$

$$R^2 = (r_{\min} - m)^2 + n^2 \quad (46)$$

Using (45) and (46), we can obtain

$$R^2 = r_{\min}^2 - 2r_{\min}(r_e + r_{\min})(1 - \cos \psi) + \frac{A_{\text{cap}}}{\pi}. \quad (47)$$

Using the geometric identity for surface area of any spherical cap, we can write  $A_{\text{cap}} = 2\pi(r_e + r_{\min})^2(1 - \cos \psi)$ . Substituting  $A_{\text{cap}}$  in (47), we get

$$R^2 = r_{\min}^2 + \frac{A_{\text{cap}}}{\pi} \left(1 - \frac{r_{\min}}{r_e + r_{\min}}\right) \quad (48)$$

Similarly at  $\theta_e = \theta_0$ , a spherical cap of surface area  $A_{\text{vis}}$  is formed by the all the visible satellites at distance less than or equal to maximum distance  $r_{\max}$  from the user. Hence similar to (48), for  $R = r_{\max}$ , we can write

$$r_{\max}^2 = r_{\min}^2 + \frac{A_{\text{vis}}}{\pi} \left(1 - \frac{r_{\min}}{r_e + r_{\min}}\right). \quad (49)$$

or

$$A_{\text{vis}} = \frac{\pi}{r_e} (r_{\max}^2 - r_{\min}^2) (r_e + r_{\min}). \quad (50)$$

*Step 2:* From Fig. 2, the CDF of the surface area of the spherical cap formed by satellites at a random distance less than or equal to  $R$  from a user is

$$F_{A_{\text{cap}}}(x) = \frac{x}{A_{\text{vis}}}. \quad (51)$$

*Step 3:* Using the relationship between  $A_{\text{cap}}$  and  $R$  as derived in (48), the CDF of the distance  $F_R(r)$  can be written as

$$\begin{aligned} F_R(r) &= \mathbb{P}(R \leq r) = \mathbb{P}(R^2 \leq r^2) \\ &= \mathbb{P}\left(r_{\min}^2 + \frac{A_{\text{cap}}}{\pi} \left(1 - \frac{r_{\min}}{r_e + r_{\min}}\right) \leq r^2\right) \\ &= \mathbb{P}\left(A_{\text{cap}} \leq \frac{\pi(r^2 - r_{\min}^2)}{1 - \frac{r_{\min}}{r_e + r_{\min}}}\right) \\ &= \frac{\pi(r^2 - r_{\min}^2)}{A_{\text{vis}} \left(1 - \frac{r_{\min}}{r_e + r_{\min}}\right)}. \end{aligned} \quad (52)$$

Using (50) in (52), we can write

$$F_R(r) = \frac{r^2 - r_{\min}^2}{r_{\max}^2 - r_{\min}^2}, \text{ for } r_{\min} \leq r \leq r_{\max} \quad (53)$$

where the  $r_{\max}$  is given by (44). The corresponding PDF can be found by differentiating (53) with respect to  $r$ .

## APPENDIX B

PROOF FOR SUCCESS PROBABILITY OF  $K_{\text{vis}}$ 

The success probability is given by the ratio of the surface area of the spherical cap region where a visible satellite can lie to the total surface area of the sphere. It can be written as

$$\mathcal{P} = \frac{A_{\text{vis}}}{4\pi (r_e + r_{\min})^2} \quad (54)$$

Using (50) in (54), we can write

$$\begin{aligned} \mathcal{P} &= \frac{\pi(r_{\max}^2 - r_{\min}^2)(r_e + r_{\min})}{4\pi r_e (r_e + r_{\min})^2} \\ &= \frac{r_{\max}^2 - r_{\min}^2}{4r_e (r_e + r_{\min})} \end{aligned} \quad (55)$$

## APPENDIX C

DERIVATION OF  $\mathbb{E}[r_{us}^{-\alpha} H_{us}]$ 

Since  $H_{us}$  and  $R_{us}$  are independent,  $\mathbb{E}[r_{us}^{-\alpha} H_{us}]$  can be written as

$$\mathbb{E}[r_{us}^{-\alpha} H_{us}] = \mathbb{E}[r_{us}^{-\alpha}] \mathbb{E}[H_{us}]. \quad (56)$$

Using (2) and (10),  $\mathbb{E}[r_{us}^{-\alpha}]$  and  $\mathbb{E}[H_{us}]$  can be solved as

$$\begin{aligned} \mathbb{E}[r_{us}^{-\alpha}] &= \int_{r_{\min}}^{r_{\max}} r_{us}^{-\alpha} f_R(r_{us}) dr_{us} \\ &= \begin{cases} \frac{2(r_{\max}^{2-\alpha} - r_{\min}^{2-\alpha})}{(2-\alpha)(r_{\max}^2 - r_{\min}^2)} & \text{for } \alpha \neq 2, \\ \frac{2}{r_{\max}^2 - r_{\min}^2} \ln\left(\frac{r_{\max}}{r_{\min}}\right) & \text{for } \alpha = 2, \end{cases} \end{aligned} \quad (57)$$

and

$$\begin{aligned} \mathbb{E}[H_{us}] &= \int_0^{\infty} h_{us} f_{H_i}(h_{us}) dh_{us} \\ &= \sum_{\kappa=0}^{m_i-1} \frac{\alpha_i \zeta(\kappa) \eta_i \Gamma(\kappa+2)}{(\beta_i - \delta_i)^{\kappa+2}}. \end{aligned} \quad (58)$$

## APPENDIX D

## NUMERICAL INTEGRATION IN (23)

The integral term in (23) can be efficiently calculated using the `vpaintegral` function of MATLAB. It uses the global adaptive quadrature technique and variable precision arithmetic to perform the integration. The speed of the execution can be traded-off with the tolerance value. Consider

$$\text{func} = M_{\gamma_{us}|r_{us}}(-t) f_R(r_{us}),$$

where  $f_R(r_{us})$  and  $M_{\gamma_{us}|r_{us}}(-t)$  are given in (10) and (22), respectively. Then, the integral term in (23) can be evaluated using

$$\begin{aligned} &\text{vpaintegral}(\text{func}, r, r_{\min}, r_{\max}, \dots \\ &\quad \text{'RelTol'}, 1e-4, \text{'AbsTol'}, 0); \end{aligned}$$

where  $r_{\min} = r_{\min}$ ,  $r_{\max} = r_{\max}$  and the integration is done for a relative tolerance of  $10^{-4}$  and the option to set the absolute tolerance is turned off.

## REFERENCES

- [1] R. Lorrain, "LoRa: Delivering internet of things capabilities worldwide," *Inside Out: Semtech's Corporate Blog*, 2022, (Accessed 15 Oct. 2022). [Online]. Available: <https://blog.semtech.com/lora-delivering-internet-of-things-capabilities-worldwide>
- [2] Z. Qu, G. Zhang, H. Cao, and J. Xie, "LEO satellite constellation for internet of things," *IEEE Access*, vol. 5, pp. 18391–18401, 2017.
- [3] 3rd Generation Partnership Project (3GPP); Technical Specification Group Radio Access Network, "Study on NB-IoT/eMTC support for Non-Terrestrial Networks (NTN) (Rel 17)," *TR 36.763*, 2021.
- [4] I. Portillo, B. G. Cameron, and E. F. Crawley, "A technical comparison of three low earth orbit satellite constellation systems to provide global broadband," *Acta Astronaut.*, vol. 159, pp. 123 – 135, 2019.
- [5] M. Centenaro, C. E. Costa, F. Granelli, C. Sacchi, and L. Vangelista, "A survey on technologies, standards and open challenges in satellite IoT," *IEEE Commun. Surv. Tutor.*, vol. 23, no. 3, pp. 1693–1720, 2021.
- [6] M. Vaezi *et al.*, "Cellular, wide-area, and non-terrestrial IoT: A survey on 5G advances and the road toward 6G," *IEEE Commun. Surv. Tutor.*, vol. 24, no. 2, pp. 1117–1174, 2022.
- [7] N. A. J. Fraire, S. Céspedes, "Direct-to-satellite IoT - a survey of the state of the art and future research perspectives: Backhauling the IoT through LEO satellites," *ADHOC-NOW: Ad-Hoc, Mobile, and Wireless Networks*, pp. 241–258, 2019.
- [8] J. A. Fraire, S. Henn, F. Dovis, R. Garello, and G. Taricco, "Sparse satellite constellation design for LoRa-based direct-to-satellite internet of things," in *IEEE Global Commun. Conf. GLOBECOM*, 2020, pp. 1–6.
- [9] An ultra-low cost sensor service for small amounts of data, *Lacuna Space*, (Accessed 15 Oct. 2022). [Online]. Available: <https://lacuna.space/>
- [10] Astronode development kit, *Astrocast*, (Accessed 15 Oct. 2022). [Online]. Available: <https://www.astrocast.com/>
- [11] OG2 Satellite IoT modems, *ORBCOMM*, (Accessed 15 Oct. 2022). [Online]. Available: <https://www.orbcomm.com/en/partners/connectivity/satellite/og2>
- [12] K. J. R. Liu, A. K. Sadek, W. Su, and A. Kwasinski, *Cooperative Communications and Networking*. Cambridge University Press, 2008, ch. 4.
- [13] M. R. Bhatnagar and A. M.K., "Performance analysis of AF based hybrid satellite-terrestrial cooperative network over generalized fading channels," *IEEE Commun. Lett.*, vol. 17, no. 10, pp. 1912–1915, 2013.
- [14] D. B. da Costa and S. Aissa, "Performance of cooperative diversity networks: Analysis of amplify-and-forward relaying under equal-gain and maximal-ratio combining," in *2009 IEEE Int. Conf. on Commun.*, 2009, pp. 1–5.
- [15] N. H. Vien and H. H. Nguyen, "Performance analysis of fixed-gain amplify-and-forward relaying with MRC," *IEEE Trans. on Veh. Technol.*, vol. 59, no. 3, pp. 1544–1552, 2010.
- [16] S. S. Soliman, "MRC and selection combining in dual-hop AF systems with rician fading," in *Int. Conf. on Comput. Eng. & Syst. (ICCES)*, 2015, pp. 314–320.
- [17] A. Iqbal and K. Ahmed, "A hybrid satellite-terrestrial cooperative network over non identically distributed fading channels," *J. of Commun.*, vol. 6, pp. 581–589, 2011.
- [18] H. A. Suraweera, H. K. Garg, and A. Nallanathan, "Performance analysis of two hop amplify-and-forward systems with interference at the relay," *IEEE Commun. Lett.*, vol. 14, no. 8, pp. 692–694, 2010.
- [19] H. A. Suraweera, D. S. Michalopoulos, R. Schober, G. K. Karagiannidis, and A. Nallanathan, "Fixed gain amplify-and-forward relaying with co-channel interference," in *Int. Conf. on Commun. (ICC)*, 2011, pp. 1–6.
- [20] O. Abbasi, A. Ebrahimi, and N. Mokari, "NOMA inspired cooperative relaying system using an AF relay," *IEEE Wireless Commun. Lett.*, vol. 8, no. 1, pp. 261–264, 2019.
- [21] A. Argyriou, "Multi-source cooperative communication with opportunistic interference cancelling relays," *IEEE Trans. on Commun.*, vol. 63, no. 11, pp. 4086–4096, 2015.
- [22] J. M. de Souza Sant'Ana, A. Hoeller, R. D. Souza, H. Alves, and S. Montejo-Sánchez, "LoRa performance analysis with superposed signal decoding," *IEEE Wireless Commun. Lett.*, vol. 9, no. 11, pp. 1865–1868, 2020.
- [23] U. Noreen, L. Clavier, and A. Bounceur, "LoRa-like CSS-based PHY layer, capture effect and serial interference cancellation," in *24th Eur. Wireless Conf.*, 2018, pp. 1–6.
- [24] N. Okati, T. Riihonen, D. Korpi, I. Angervuori, and R. Wichman, "Downlink coverage and rate analysis of low earth orbit satellite constellations using stochastic geometry," *IEEE Trans. Commun.*, vol. 68, no. 8, pp. 5120–5134, 2020.

- [25] C. C. Chan, B. Al Homssi, and A. Al-Hourani, "A stochastic geometry approach for analyzing uplink performance for IoT-over-satellite," in *IEEE Int. Conf. Commun.*, 05 2022.
- [26] H. Lin, C. Zhang, Y. Huang, R. Zhao, and L. Yang, "Fine-grained analysis on downlink LEO satellite-terrestrial mmwave relay networks," *IEEE Wireless Commun. Lett.*, vol. 10, no. 9, pp. 1871–1875, 2021.
- [27] A. K. Dwivedi, S. Praneeth Chokkarapu, S. Chaudhari, and N. Varshney, "Performance analysis of novel direct access schemes for LEO satellites based IoT network," in *IEEE 31st Annu. Int. Symp. Pers., Indoor, Mobile, Radio Commun. (PIMRC)*, 2020, pp. 1–6.
- [28] S. Tegos, P. Diamantoulakis, A. Lioumpas, P. Sarigiannidis, and G. Karagiannidis, "Slotted ALOHA with NOMA for the next generation IoT," *IEEE Trans. on Commun.*, vol. 68, no. 10, pp. 6289–6301, 2020.
- [29] A. Abdi, W. C. Lau, M. Alouini, and M. Kaveh, "A new simple model for land mobile satellite channels: first- and second-order statistics," *IEEE Trans. Wireless Commun.*, vol. 2, no. 3, pp. 519–528, 2003.
- [30] V. Singh, P. K. Upadhyay, and M. Lin, "On the performance of NOMA-assisted overlay multiuser cognitive satellite-terrestrial networks," *IEEE Wireless Commun. Lett.*, pp. 1–1, 2020.
- [31] I. Gradshteyn and I. Ryzhik, "Tables of integrals, series and products," *New York: Academic Press*, 2000.
- [32] E. Aboutanios, "Frequency estimation for low earth orbit satellites," Ph.D. dissertation, Fac. of Eng. (Telecommun. Group), Univ. of Technol., Sydney, 2002.
- [33] V. Singh and P. K. Upadhyay, "Exploiting FD/HD cooperative-NOMA in underlay cognitive hybrid satellite-terrestrial networks," *IEEE Trans. on Cogn. Commun. and Netw.*, vol. 8, no. 1, pp. 246–262, 2022.
- [34] Semtech Corp., *AN1200.22 LoRa Modulation Basics*. Camarillo, CA, USA, 2015, (Accessed 15 Oct. 2022). [Online]. Available: <https://www.frugalprototype.com/wp-content/uploads/2016/08/an1200.22.pdf>
- [35] M. Aldababsa, M. Toka, S. Gökceli, G. Karabulut Kurt, and O. Kucur, "A tutorial on non-orthogonal multiple access for 5G and beyond," *Wireless Commun. Mob. Comput.*, vol. 2018, 06 2018.
- [36] Y.-C. Ko, M.-S. Alouini, and M. Simon, "Outage probability of diversity systems over generalized fading channels," *IEEE Trans. Commun.*, vol. 48, no. 11, pp. 1783–1787, 2000.
- [37] N. I. Miridakis, D. D. Vergados, and A. Michalas, "Dual-hop communication over a satellite relay and shadowed rician channels," *IEEE Trans. Veh. Technol.*, vol. 64, no. 9, pp. 4031–4040, 2015.